RSC Advances

PAPER

View Article Online
View Journal | View Issue



Cite this: *RSC Adv.*, 2019, **9**, 38414

# Synthesis of Au-decorated three-phase-mixed $TiO_2$/phosphate modified active carbon nanocomposites as easily-recycled efficient photocatalysts for degrading high-concentration 2,4-DCP†

Sharafat Ali, Zhijun Li,* Wajid Ali, Ziqing Zhang, Mingzhuo Wei, Yang Qu and Liqiang Jing*

It is of great significance to fabricate easily-recycled $TiO_2$ photocatalysts with high activity. Herein, dominant-anatase three-phase (anatase/rutile/brookite)-mixed nanosized $TiO_2$ with high photocatalytic activity for degrading a high-concentration of 2,4-DCP has been synthesized *via* a hydrothermal process with HCl as a phase-directing agent, and interestingly the apparent photoactivity could be greatly improved by decorating Au nanoparticles and then coupling phosphate-treated active carbon. The amount-optimized nanocomposite displays ~12-fold enhancement in degradation rate constant (*k*) compared to anatase $TiO_2$. Based on the steady-state surface photovoltage spectra, fluorescence spectra related to the produced ·OH amount, temperature-programmed desorption and $O_2$ electrochemical reduction curves, it is confirmed that the exceptional photoactivity is mainly attributed to the greatly-enhanced charge separation from the phase-mixed composition, and from the decorated Au as electron acceptors and its promotion effects on $O_2$ activation. Moreover, the use of phosphate-modified AC as a support is also positive for efficient photocatalytic reactions by accepting electrons and concentrating the pollutants, with recyclable features. This work provides a feasible strategy to fabricate $TiO_2$-based nano-photocatalysts for degrading high-concentration pollutants to remediate the environment.

Received 11th October 2019
Accepted 18th November 2019

DOI: 10.1039/c9ra08286g

rsc.li/rsc-advances



## 1. Introduction

2,4-Dichlorophenol (2,4-DCP) is extensively used as an intermediate in the preparation of pesticides, preservatives, disinfectants, herbicides and germicides.[1,2] The generation of waste water during production and use of chlorophenolic compounds, *i.e.* 2,4-DCP is ultimately released into the environment as a serious pollutant.[3,4] The dissolved 2,4-DCP is promptly absorbed through skin into the body and it can be fatal, since it may cause endocrine disruption, liver damage and failure of several other organs. Thus, it is very indispensable to remove the noxious 2,4-DCP from polluted water so as to protect the safety regarding drinking water, which is closely associated with our health.[5,6] Among various techniques, the photocatalytic technique has long been considered as one of the most innovative and scalable approaches owing to its modest cost and environmental benignity, *etc.* compared with traditional physical and biological treatment methods.[7–9]

Among the plentiful semiconductors investigated, $TiO_2$ unquestionably is an appealing semiconductor photocatalyst due to its desirable properties such as modest cost, strong oxidizing power and environmentally benign.[10–13] $TiO_2$ mainly exists in three distinct phases, anatase, rutile and brookite.[14,15] Among these three phases, anatase phase is considered as the most active phase and is therefore extensively used in the variety of photocatalytic applications.[16] Nevertheless, the efficiency of $TiO_2$ is still restricted by undesirable recombination of electron–hole pairs.[17–19] Among the various modification strategies, constructing of heterojunction is one of the most promising strategy to enhance the photogenerated charges separation of $TiO_2$, like $SrTiO_3/TiO_2$,[20] $ZnO/TiO_2$,[21] *etc.* Remarkably, homogeneous heterophase of $TiO_2$, like rutile/anatase, the commercial Degussa P25, is the most widely studied $TiO_2$ with good photoactivities attributable to high charge separation,[15,22] whereas fewer studies have been made on anatase/brookite and brookite/rutile solids, especially for the three-phase-mixed one.[23] As of late, it has been demonstrated that brookite has

*Key Laboratory of Functional Inorganic Materials Chemistry (Ministry of Education), School of Chemistry and Materials Science, International Joint Research Center for Catalytic Technology, Heilongjiang University, Harbin 150080, PR China. E-mail: 2018011@hlju.edu.cn; jinglq@hlju.edu.cn*

† Electronic supplementary information (ESI) available. See DOI: 10.1039/c9ra08286g

the most negative conduction band among the three $TiO_2$ phases, which leads to more energetically favourable for reduction reactions.[24,25] Therefore, $TiO_2$ with phase-mixed junctions (anatase/brookite/rutile) has the potential to become a better heterogeneous photocatalyst than pure single phase. Besides that, in order to further improve the charge separation and catalytic ability, it is an effective strategy to couple with noble metals such as Au, Ag, *etc.*[26–28] To this end, it is much feasible to decorate noble metal Au to improve the photoactivity of phase-mixed $TiO_2$ with high activity.

Nonetheless, the high adsorption of pollutants and recyclability are the key issues to determine the photocatalytic performance of the photocatalyst. As for those purpose, it is a viable strategy to couple with some other substrates, such as carbon nanotube, graphene and activated carbon (AC) *etc.* Among those substrates, AC is considered as the most suitable substrate because of its low cost, high surface area, porous structure, strong adsorption for pollutants and being recycled in recent years.[29–33] As reported in our previous works, it serves not only as high adsorption agents but also as collectors to accept electrons to effectively hinder photogenerated charge recombination.[20] Noticeably, the interfacial contact between the constructed components is one of the most important factors for activities and stability of the photocatalyst. In our previous work, the phosphate with multiple hydroxyl groups could be taken as a bridge to connect different semiconductor nano-oxides with surface hydroxyl groups by a chemical process, so as to improve the stability of the composite. Meanwhile, the phosphate bridge is beneficial to promote the charge transfer between the constructed components, along with the promoted adsorption of $O_2$ during the photocatalytic degradation of organic pollutions.[33,34]

Thus, the objective of this study is to prepare three-phase-mixed $TiO_2$ based nano-photocatalyst with high charge separation for effectively degrading high-concentration 2,4-DCP pollutant. It is clearly shown that the improved photocatalytic activities are attributed to the greatly-enhanced charge separation from the phase-mixed $TiO_2$, and from the decorated Au as electron acceptors and promotion effects on $O_2$ activation, and to the phosphate-modified active carbon to increase adsorption of pollutants, enhance charge separation as well as to improve the interfacial contact between the constructed components. Another feature of this work is the good recycling performance of resulting hybrid photocatalyst in the wastewater treatment. This work can provide a convenient method to modulate the phase components of $TiO_2$, and also provide effective strategies to improve the photocatalytic activities of phase-mixed $TiO_2$ for environmental remediation.

# 2. Experimental part

## 2.1. Materials and methods

All the chemical reagents were obtained from commercial sources as guaranteed-grade reagents and used without further treatment. Deionized water was used throughout the experiments.

## 2.2. Synthesis of the samples

**2.2.1. Synthesis of Au/phase-mixed $TiO_2$ nanocomposites.** Synthesis of phase-mixed $TiO_2$ nanoparticles: phase-mixed $TiO_2$ (MTO) was synthesized by mixing 5 mL $Ti(OBu)_4$ and 5 mL anhydrous ethanol under vigorous stirring, and then the solution was slowly dropwise added into a mixture containing 20 mL ethanol, 5 mL deionized water and different amounts of HCl (1, 2, 3 and 4 mL) solution to form a transparent solution. Afterward, the resulting solution was transferred to a Teflon-lined stainless 100 mL capacity and was heated at 160 °C for 6 h. After cooling to room temperature naturally, the obtained precipitates were rinsed several times with deionized water and absolute ethanol, dried in an oven at 80 °C and finally calcined at 450 °C (5 °C $min^{-1}$) for 2 h. These samples were represented by *X*MTO where "*X*" represents volume of HCl added and MTO represents phase-mixed $TiO_2$. The same procedure was applied by adding $HNO_3$ instead of HCl to synthesize anatase $TiO_2$, denoted as ATO.

**2.2.2. Synthesis of Au/MTO composites.** Different mass percent (0.5, 1.0, 2.0, and 3.0%) of Au NPs were loaded on the surface of 3MTO by deposition–precipitation (DP) method using $HAuCl_4 \cdot 4H_2O$ as a starting material. For each sample, 0.5 g of 3MTO were dispersed into 500 mL water containing the necessity amount of $HAuCl_4 \cdot 4H_2O$. The mixed solution was adjusted to pH = 7 by using 1 mM NaOH solution and kept at 80 °C in water bath under stirring for 3 h. Finally, the obtained precipitate was rinsed with deionized water and absolute ethanol in turn, and then dried at 80 °C and calcined at 300 °C (5 °C $min^{-1}$) for 0.5 h. The obtained samples were represented by *Y*Au/3MTO, where "*Y*" represents mass ratio percentage of Au to MTO.

**2.2.3. Synthesis of MTO/10AC nanocomposites.** 1 g of the as-prepared 3MTO sample was dispersed into a mixture containing 20 mL absolute ethanol, 5 mL deionized water and 1 mL of $HNO_3$ (70%). Then 0.1 g AC was put in the mixture under vigorous stirring for 1 h. The sample was washed with deionized water and ethanol and dried in oven at 80 °C and finally calcined at 350 °C (5 °C $min^{-1}$) for 2 h. The same procedure was applied to coupled AC to anatase $TiO_2$ and Au/MTO composites.

**2.2.4. Synthesis of (2Au/3MTO)/P-10AC.** In a typical procedure, 1 g of AC was mixed with 50 mL phosphate solution of different concentrations (0.0001, 0.0002, 0.0003 and 0.0005 M) under vigorous stirring for 1 h. The obtained products were washed several times with deionized water and absolute ethanol, dried in an oven at 80 °C and calcined at 350 °C (5 °C $min^{-1}$) for 2 h. The obtained powders were denoted by *Z*P-AC. Subsequently, 1 g of 2Au/3MTO was mixed with 0.1 g of each *Z*P-AC sample in a mixture containing 20 mL ethanol, 5 mL water and 1 mL $HNO_3$ (70%) under vigorous stirring for 1 h, dried at 80 °C and finally calcined at 350 °C (5 °C $min^{-1}$) for 2 h. The obtained samples were represented by (2Au/3MTO)/*Z*P-AC. For *Z*P-AC, "P" stands for phosphoric acid and "*Z*" for its concentrations of used solution (0.0001, 0.0002, 0.0003 and 0.0005 M).

### 2.3. Characterization of materials

Different techniques were used for the characterization of the as-prepared nanocomposites. The crystal structures of the as-prepared nanocomposites were confirmed with the help of XRD (Bruker D8, Germany) by using Cu K$\alpha$ radiation source ($\alpha =$ 1.54056 Å), operated at an accelerating voltage of 30 kV and an emission current of 20 mA was used. The UV-vis diffuse reflectance spectra (DRS) were recorded with a Model Shimadzu UV-2550 spectrometer. Fourier transform infrared (FT-IR) spectra were obtained at the range of 500–4000 $cm^{-1}$ using KBr as diluents in order to measure various bonds and impurities present in the prepared nanocomposites. The morphology of the as-prepared nanocomposites was investigated using a JEOL JEM-2010 transmission electron microscope (TEM), with an acceleration voltage of 200 kV. The BET specific surface area of the as-prepared nanocomposites were carried out by $N_2$ adsorption–desorption method at the temperature of liquid nitrogen Micromeritics Tristar II 3020 system Atlanta, GA, USA, after being degassed at 150 °C for 10 h. The fluorescence spectra (FS) were measured with a spectrofluoro-photometer (Perkin-Elmer LS55) at excitation wavelength of 390 nm. The surface photovoltage spectroscopy (SPS) measurement of the samples was carried out with a home-built equipped with a lock-in amplifier (SR830) and synchronized with a light chopper (SR540).

### 2.4. Evaluation of temperature-programmed desorption (TPD)

The temperature-programmed desorption (TPD) of $O_2$ were made *via* using home built equipped. Every sample (50 mg) was first pre-treated to 300 °C (10 °C $min^{-1}$) under helium (He) gas (25–30 mL $min^{-1}$) in order remove gas molecules and adsorbed moisture. Afterward, pure He gas was passed through each sample in order to remove weakly adsorbed $O_2$. Finally, the TPD curve was recorded up to 700 °C (10 °C $min^{-1}$).

### 2.5. Electrochemical reduction measurement

The electrochemical reduction experiments were made in a three-electrode cell with a platinum wire (99.9%) as the counter electrode, a Ag/AgCl (satd KCl) electrode as the reference electrode, the prepared film electrodes as the working electrode, and the 0.5 M $NaClO_4$ solution as the electrolyte. Subsequently, high-purity gas ($O_2$ or $N_2$) was used to bubble through the electrolyte before and during the experiments. The electrochemical reduction experiments of $O_2$ and $N_2$ were measured in dark. Applied potentials were controlled by a commercial computer-controlled potentiostat (AUTOLABPG STAT).

### 2.6. Evaluation of hydroxyl radical ($\cdot$OH) amount

Hydroxyl radical measurement was carried out in quartz cell containing 50 mL of the as-prepared 0.001 M coumarin aqueous solution and 0.025 g of each sample. The reactor was irradiated under UV-vis light irradiation using a source of 300 W high-pressure xenon lamp under magnetic stirring for 1 h. After 1 h irradiation, a certain amount of each sample was taken in a Pyrex glass cell for the fluorescence measurement of 7-hydroxycoumarin under excitation wavelength of 390 nm and 460 nm emission wavelengths through a spectrofluorometer (Perkin-Elmer LS55).

### 2.7. Evaluation of photocatalytic activities for 2,4-DCP degradation

Photocatalytic activities of the as-prepared samples were assessed by degrading 2,4-DCP at room temperature under UV-vis light irradiation. In each experiment, 0.025 g photocatalyst was added to 2,4-DCP solution (100 mg $L^{-1}$, 100 mL) and stirred in dark for 30 min to ensure adsorption–desorption equilibrium. Subsequently, the suspension was irradiated under UV-vis light (300 W Xe-lamp) irradiation. During the irradiation period, samples were taken from the suspension at regular intervals of time and analysed by Model Shimadzu UV-2550 Spectrophotometer (Kyoto, Japan).

## 3. Results and discussion

### 3.1. Synthesis of phase-mixed $TiO_2$

The crystallinity and phase structures of the as-prepared nanocomposites were elucidated through X-ray diffraction (XRD) and the effect of varying amounts of HCl on the phase structures was investigated. Fig. 1A shows XRD patterns of the anatase $TiO_2$ (ATO) and phase-mixed $TiO_2$ (MTO). The observed peak clearly showed phase-mixed of $TiO_2$ that consists of anatase, rutile and brookite nanocrystals. As increasing the amount of HCl, relative percentage of anatase is decreasing, while rutile and brookite percentage is increasing. The possible formation mechanisms of $TiO_2$ with various phases could be well explained by referring to the works reported by Agnès Pottier *et al.* The complex $Ti(OH)_2(Cl)_2(OH_2)_2$ would probably be the precursor of the brookite and rutile phase, and a high concentration of chloride ions in the thermolysis medium of titanium is be necessary for the formation of brookite and also to avoid recrystallisation of brookite into rutile during ageing in suspension. Meanwhile the presence of chloride ions is also necessary to stabilize the brookite in suspension.[35] The content of different phases and the BET analysis of *X*MTO nanocomposites are shown in Table S1.† The as-prepared 1MTO, 2MTO, 3MTO and 4MTO nanocomposites present large BET specific surface areas of 77.7, 87.15, 124.2 and 98.0 $m^2\ g^{-1}$, respectively, which means 3MTO have most active sites for photocatalytic reactions than others. The optical absorption properties of the as-prepared ATO and *X*MTO nanocomposites were characterized by UV-vis diffusion reflectance spectra. It can be seen from Fig. S1A,† that there are slightly changes in the absorption edges of *X*MTO compared to ATO, due to the formation of rutile. The morphological and structural features of 3MTO were investigated by transmission electron microscopy (TEM) and high-resolution TEM (HRTEM), as shown in Fig. 1B. In the HRTEM image of 3MTO, the distance between each lattice fringes were measured and identified as the different phases of $TiO_2$. The fringe widths of 0.332 nm, 0.238 nm and

 

0.29 nm can be used to confirm the dominance of (101), (110) and (200) planes of anatase, rutile and brookite structure, respectively.[36,37] While the size of 3MTO is in the range of 8–10 nm. It is well known that the photogenerated charge properties greatly affect the photocatalytic performance, and surface photovoltage spectroscopy (SPS) is a promising technique used to reveal the separation of excited electron–hole pairs of semiconductor materials. Generally speaking, strong SPS signal shows high charge separation and *vice versa*.[38] It can be seen from Fig. 1C, that ATO shows a rather low SPS response compared to MTO, which suggested that the phase mixing is a good way to enhance the charge separation. Especially, the 3MTO presented the highest SPS response among phase-mixed $TiO_2$ samples. This is credited to the efficient separation of the photogenerated electron–hole pairs due to appropriate percentage of brookite in the nanocomposite.

In order to further verify the charge separation, it is meaningful to test the ·OH amount through the wide-used coumarin fluorescent method as a highly sensitive technique. The FS spectra related to the produced ·OH amounts were employed in which the coumarin could readily react with the formed ·OH radicals and produce luminescent 7-hydroxy-coumarin.[20] In Fig. S1B,† the 3MTO nanocomposite shows the highest fluorescent response among all the nanocomposites, corresponding to the most efficient charge separation. This is good consistent with the SPS results.

The photocatalytic activities of ATO and MTO nanocomposites were assessed by degrading 2,4-DCP under UV-vis light irradiation as shown in Fig. 1D. It can be clearly shown that all MTO nanocomposites shows rather higher photocatalytic activity than ATO. As expected, all the MTO nanocomposites exhibits improved photocatalytic activities to degrade high-concentration pollutant 2,4-DCP. It is sure that the improved photocatalytic activities are mainly attributed to the optimized BET specific surface area and proper phase composition which efficiently enhances charge separation, especially for the 3MTO nanocomposite achieving about 90% 2,4-DCP degradation rate in 4 h.

### 3.2. Modification of Au onto MTO

The XRD patterns of *X*MTO has not been disturbed after Au modification (Fig. S2A†), and there is no peak appeared corresponding to Au for the *Y*Au/3MTO nanocomposites, owing to tiny amount of the decorated Au with high dispersion. To further clarify the effect of decorated Au in the nanocomposites, the TEM and HRTEM were carried out for the 2Au/3MTO nanocomposite as shown in Fig. 2A. It is obvious that the lattice fringes with *d*-spacing 0.24 nm corresponds to Au,[39] which have closed contact to the surface of MTO (anatase $d_{101}$ = 0.332 nm, rutile $d_{101}$ = 0.238 nm and brookite $d_{101}$ = 0.29 nm). Apparently, the Au didn't change the particle size of 3MTO nanocomposite. UV-vis DRS spectra (Fig. 2B) show that the bandgap of 3MTO is barely changed after decorating Au, while a remarkable optical absorption appears in the visible-light region probably due to the plasmonic effect of nanosized Au. In order to explore the charge separation of *Y*Au/3MTO nanocomposites, SPS spectra were evaluated as shown in Fig. 2C. Normally, the SPS response is in direct proportion to the charge separation. It is clearly seen, as the amount of decorated Au increases, the intensity of SPS response becomes gradually stronger, especially for the 2Au/3MTO nanocomposite. To further explore and support the enhanced charge separation, the fluorescence method is applied to measure the ·OH amounts, as shown in Fig. S2B.† The 2Au/3MTO nanocomposite produces the largest amount of ·OH among all the modified nanocomposites, indicating that Au is beneficial for the charge transfer, which is in good agreement with the SPS results. Accordingly, the photocatalytic activities of Au modified 3MTO for 2,4-DCP degradation were evaluated under UV-vis light

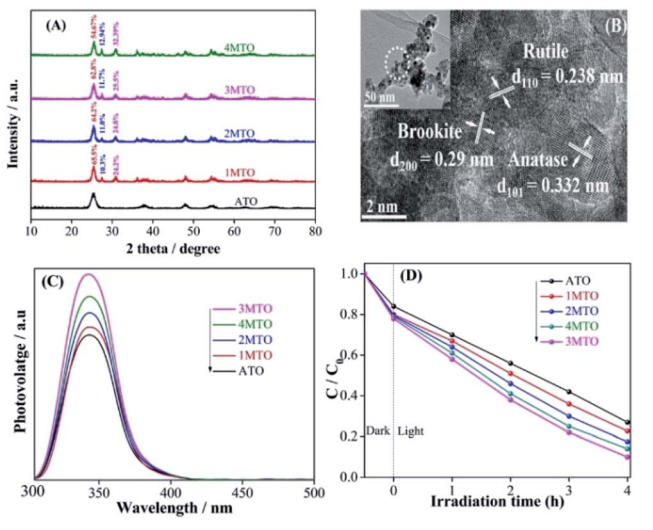


Fig. 1 XRD patterns of ATO and *X*MTO (A), TEM and HRTEM images of 3MTO (B), DRS spectra (C) and photocatalytic activities of 2,4-DCP degradation under UV-vis light irradiation (D) of ATO and *X*MTO. (*X* stands for 1, 2, 3 and 4 mL of HCl, ATO for anatase $TiO_2$ and MTO for phase-mixed $TiO_2$). It is the same elsewhere unless stated.

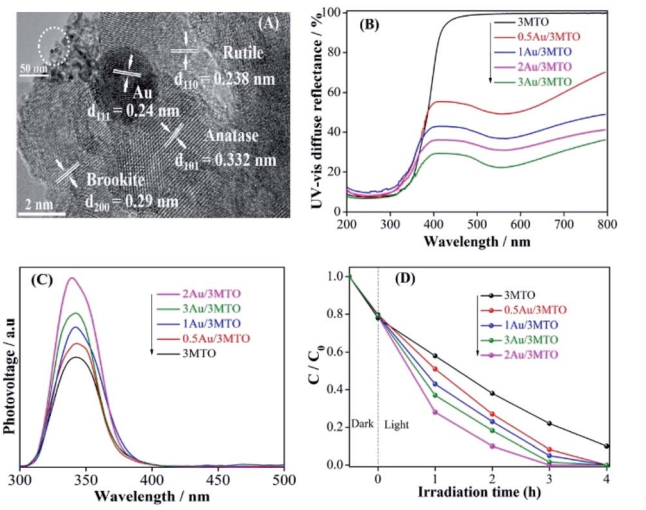


Fig. 2 TEM and HRTEM of 2Au/3MTO (A), DRS spectra (B), SPS responses (C), and photocatalytic activity (D) of 3MTO and *Y*Au/3MTO for 2,4-DCP degradation. (*Y* stands for mass percentage of Au to 3MTO). It is the same elsewhere unless stated.

irradiation, as shown in Fig. 2D. The complete degradation of 2,4-DCP is achieved for 2Au/3MTO in 3 h. The improved activity is attributed to the decorated Au, which enhances charge separation as well as serves as a co-catalyst to provide active sites for inducing reduction reactions.

Unexpectedly, the *Y*Au/3MTO has a negligible activity under visible-light irradiation for high-concentration pollutant, indicating that SPR absorption of supported Au particles didn't contribute to the degradation for high-concentration pollutants (Fig. S2C†). While the 2Au/3MTO nanocomposite shows a poor activity under visible-light irradiation for the low-concentration 2,4-DCP, suggesting that Au mainly serve as co-catalyst for 2,4-DCP degradation (Fig. S2D†).

### 3.3. Coupling of phosphate treated AC with 2Au/3MTO

The crystallinity and phase purity of 2Au/3MTO have not been disturbed after coupling AC and different amounts of $H_3PO_3$-AC (P-AC), and the results of XRD patterns are shown in Fig. 3A. It is clear that the spherical particles of 2Au/3MTO with 15–30 nm diameter were tightly adhered to the modified 3P-AC support by means of the SEM images in Fig. S3A and B.† To further investigate the interfacial bonding of phosphate groups and AC, the FTIR spectra were performed, as shown in Fig. S4A.† Noteworthily, there are two peaks observed in the P-AC samples, one is about 1020–1080 $cm^{-1}$ assigned to the characterized of phosphate groups, resulting from the P–O mode,[40] and another is at about 1620–1800 $cm^{-1}$ assigned to the hydroxyl groups.[41] Thus, it is confirmed that phosphate groups have successfully been modified on the AC surface. The UV-vis DRS of the fabricated nanocomposites were measured and shown in Fig. S4B.† The optical absorbance of 2Au/3MTO remains unchanged after coupling with AC and different amounts of P-AC. The charge separation of the as-prepared (2Au/3MTO)/10AC and (2Au/3MTO)/*Z*P-10AC nanocomposites are analysed by SPS spectra. As shown in Fig. 3B, a proper amount of AC and *Z*P-AC coupling to 2Au/3MTO is favourable for charge separation, and the (2Au/3MTO)/3P-10AC nanocomposite exhibits strongest SPS response among all the modified nanocomposites. This is further supported by the produced ·OH amount as shown in Fig. S4C.†

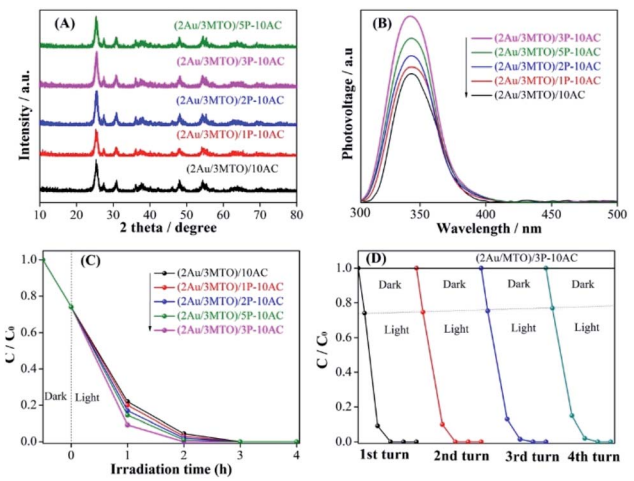


Fig. 3 XRD patterns (A), SPS response (B), photocatalytic activity (C) of (2Au/3MTO)/10AC and (2Au/3MTO)/*Z*P-10AC and stability test of (2Au/3MTO)/3P-10AC for 2,4-DCP degradation under UV-vis light irradiation (D). P means $H_3PO_4$ and *Z* in (2Au/3MTO)/*Z*P-10AC shows the molarities (0.0001, 0.0002, 0.0003 and 0.0005 M) of $H_3PO_4$ solution.

To investigate the photocatalytic activities of 2Au/3MTO after coupling with AC and *Z*P-AC for degrading high-concentration 2,4-DCP pollutant as shown in Fig. 3C. The photocatalytic activities of the as-prepared nanocomposites are greatly improved after coupling with AC and *Z*P-AC, and the (2Au/3MTO)/3P-10AC nanocomposite showed highest degradation efficiency, achieving complete degradation within 2 h. The stability is another vital index to evaluate an effective photocatalyst. Under the same experimental conditions to degrading high-concentration pollutant 2,4-DCP, (2Au/3MTO)/3P-10AC could sustain the photoactivity for 4 runs without obvious decline in photoactivity (Fig. 3D). Based on the above results, the (2Au/3MTO)/3P-10AC has excellent photocatalytic stability which make them auspicious photocatalyst for degrading high-concentration pollutant. The degradation rate constants ($k$) of ATO, 3MTO, (2Au/3MTO)/10AC and (2Au/3MTO)/3P-10AC nanocomposites are shown in Fig. S5,† which shows that (2Au/3MTO)/3P-10AC reaction is 12-time faster compared to ATO.

In order to well understand the roles of AC in the photocatalysts, the adsorption rate for 2,4-DCP over ATO, 3MTO, 2Au/3MTO and (2Au/3MTO)/10AC under dark were performed as shown in Fig. S6.† The increased dark adsorption rate of (2Au/3MTO)/10AC is mainly attributed to the 3MTO with optimized specific surface area and that of introduced AC, compared to the ATO. The XRD patterns and DRS spectra remain unchanged after modifying AC as shown in Fig. S7A and B† respectively. It is cleared that the SPS response is greatly enhanced after coupling AC, especially for the (2Au/3MTO)/10AC nanocomposite which displayed the strongest SPS based on Fig. S7C,† indicating highest charge separation. This highest charge separation is further supported by the highest amounts of ·OH produced on the resulting nanocomposites (Fig. S7D†), suggesting that AC acts as an electrons collector in order to help in transportation to the active sites. It is well consistent to the above SPS results. As expected, the photocatalytic activity of the nanocomposites is greatly improved after coupling AC, especially for (2Au/3MTO)/10AC as shown in Fig. S7E.† As demonstrated in Fig. S7F,† the (2Au/3MTO)/10AC nanocomposite exhibited superior performance over four consecutive test cycles under identical experimental conditions. These results suggest that the AC certainly plays important roles in the pollutant adsorption, photogenerated charge separation, and recycled ability of nanocomposites.

## 4. Discussion

In order to discern the photocatalytic mechanism of ATO, 3MTO, 2Au/3MTO, (2Au/3MTO)/10AC and (2Au/3MTO)/3P-10AC nanocomposites, the radical trapping experiments were conducted to elucidate the roles of reactive species that are generated during degradation of 2,4-DCP. The scavengers used in this study were isopropyl alcohol (IPA), benzoquinone (BQ), and

 

EDTA-2Na against hydroxyl radicals (·OH), superoxide anion radicals ($\cdot O_2^-$) and photogenerated holes ($h^+$), respectively.[42–44] The photocatalytic activity of ATO is almost no changed, whenever added EDTA-2Na and IPA, nevertheless an obvious inhibit is observed in the presence of BQ, suggesting that $\cdot O_2^-$ is the main active specie involve in the degradation of 2,4-DCP on ATO (Fig. S8A†). In contrast, the photocatalytic activities of 3MTO, 2Au/3MTO, (2Au/3MTO)/10AC and (2Au/MTO)/3P-10AC are mainly suppressed in the presence of IPA and a slightly decrease is observed after adding EDTA-2Na and BQ, suggesting that ·OH is dominant for the degradation of 2,4-DCP, as shown in Fig. S8B–D,† and 4A, respectively. The order of influence was $\cdot OH > h^+ > \cdot O_2^-$. As we have discussed above that the enhanced charge separation would be played a key role to improve activity of MTO for degrading high-concentration pollutant 2,4-DCP. It is well accepted that adsorbed $O_2$ could capture photogenerated electrons to form $O_2^-$, resulting enhance charge separation.[21] Thus, the adsorption of oxygen should be a prerequisite step for photocatalytic reactions, and it is understandable that an increase in the amount of adsorbed $O_2$ would be favourable for the promotion of photogenerated charge separation. Based on the results of $O_2$-TPD test, the nanocomposites have desorption peak at 600 °C in $O_2$-TPD curves (Fig. 4B), which represent for chemical adsorption of $O_2$. The (2Au/3MTO)/3P-10AC sample exhibits strongest $O_2$-TPD signals than (2Au/3MTO)/10AC and 3MTO/10AC samples. The strong $O_2$-desorption peaks of (2Au/3MTO)/3P-10AC nanocomposite implies that the surface might induce a definite extent $O_2$ adsorption which can cause by the phosphate modification. The $O_2$-TPD results recommend that phosphate modification is preferred to efficiently degrade high-concentration pollutant.

In order to further support the above results, we measured the electrochemical $O_2$ reduction of 3MTO/10AC, (2Au/3MTO)/10AC and (2Au/3MTO)/3P-10AC nanocomposites in different gas saturated environments, as shown in Fig. 4C (in $N_2$ bubbled) and Fig. 4D (in $O_2$ bubbled). It is agreeable that the detected currents in the range of −1.8 to −1.0 V against Ag/AgCl are credited $O_2$ reduction. It is noteworthy, that all the nanocomposites can activate oxygen, especially the (2Au/3MTO)/3P-10AC nanocomposite has the most obvious effect. It is beneficial for capturing photogenerated electrons and promoting charge separation so as to improve photocatalytic.

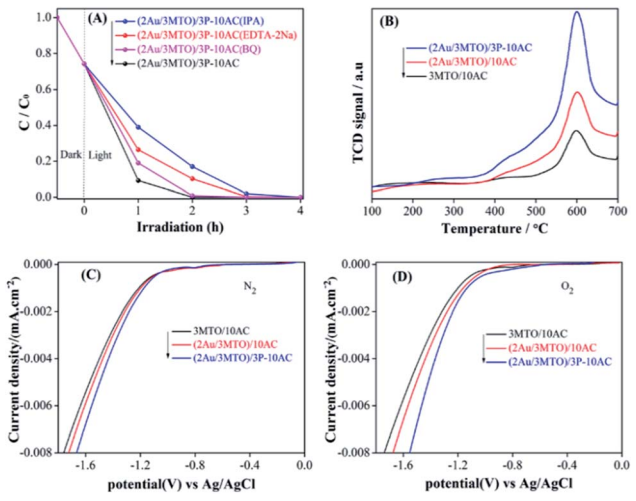


Fig. 4 Photocatalytic degradation of 2,4-DCP in the presence of IPA, BQ and EDTA-2Na under UV-vis light irradiation over (2Au/3MTO)/3P-10AC (A). $O_2$-TPD curves (B), electrochemical reduction curves in $N_2$-bubbled (C), and in $O_2$-bubbled systems (D) of 3MTO/10AC, (2Au/3MTO)/10AC and (2Au/3MTO)/3P-10AC.

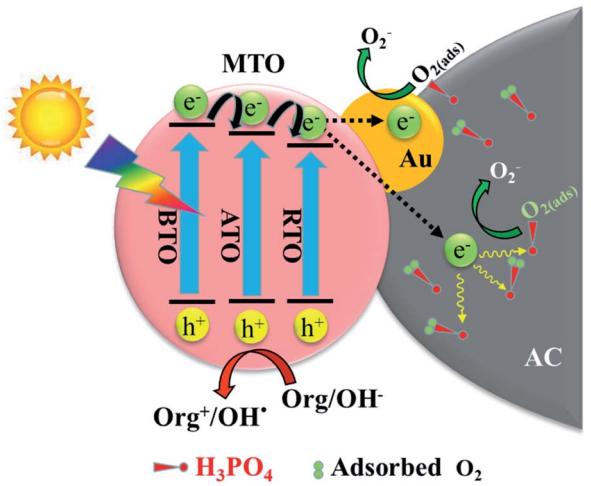


Fig. 5 Schematic of photogenerated charge separation, along with their photochemical reactions on (2Au/3MTO)/3P-10AC.

Based on the above results, a possible mechanism schematic for the photocatalytic 2,4-DCP degradation over (2Au/3MTO)/3P-10AC nanocomposites are shown in Fig. 5. After a proper amount of Au decorated onto MTO, the photogenerated electrons can thermodynamically transfer to the Au, and to be captured by the adsorbed $O_2$ to produce $\cdot O_2^-$, meanwhile producing more holes related active species participate in degradation reaction, consequently enhances the rate of photocatalytic degradation reactions, while the phosphate modified AC also hinder electron–hole recombination and facilitate the charge transfer to the sites where catalytic reaction occurs, leading to increase photocatalytic degradation of 2,4-DCP.

## 5. Conclusion

In this work, the three-phase-mixed $TiO_2$ with high photocatalytic activity has been successfully synthesized by a hydrothermal process using HCl as the phase-directing agent, and decorating Au nanoparticles and then coupling with the phosphate-treated active carbon further improve the photocatalytic activities for the 2,4-DCP degradation significantly. It is confirmed that it is attributed to the optimized specific surface area and the markedly promoted charge separation from the three-phase-mixed composites, to the decorated Au as electron acceptors as well as its promotion effects on $O_2$ activation, and to the phosphate-modified AC as the support which could accept electrons, increase $O_2$ adsorption and concentrate the pollutants, meanwhile to improve recyclability of the photocatalyst. In addition, it has been demonstrated that ·OH species

could dominate the photocatalytic degradation of 2,4-DCP on resulting phase-mixed $TiO_2$-based nano-photocatalysts due to the optimal charge separation. Naturally accepted, the comprehensive strategy of modulating the photogenerated electrons for the enhanced charge separation and then for the efficient photocatalysis to degrade organic pollutants on phase-mixed $TiO_2$-based nano-photocatalysts is extremely viable and effective. This work would provide feasible routes to synthesize phase-mixed $TiO_2$-based nano-photocatalysts for environmental remediation.

## Conflicts of interest

There are no conflicts to declare.

## Acknowledgements

Funding from NSFC (U1805255, 21905080), the program for innovative research team in Chinese universities (IRT1237), Natural science foundation of Heilongjiang Province (LH2019B017), Outstanding youth project of natural science foundation of Heilongjiang Province (YQ2019B006) and TSTAU-R2018022.

## References

1 J. Luo, Y. Wang, D. Cao, K. Xiao, T. Guo and X. Zhao, Enhanced photoelectrocatalytic degradation of 2,4-dichlorophenol by $TiO_2$/Ru-$IrO_2$ bifacial electrode, *Chem. Eng. J.*, 2018, **343**, 69–77.

2 I. A. Witońska, M. J. Walock, M. Binczarski, M. Lesiak, A. V. Stanishevsky and S. Karski, Pd-Fe/$SiO_2$ and Pd-Fe/$Al_2O_3$ catalysts for selective hydrodechlorination of 2,4-dichlorophenol into phenol, *J. Mol. Catal. A: Chem.*, 2014, **393**, 248–256.

3 A. Zada, Y. Qu, S. Ali, N. Sun, H. Lu, R. Yan, X. Zhang and L. Jing, Improved visible-light activities for degrading pollutants on $TiO_2$/g-$C_3N_4$ nanocomposites by decorating SPR Au nanoparticles and 2,4-dichlorophenol decomposition path, *J. Hazard. Mater.*, 2018, **342**, 715–723.

4 G. Jiang, K. Wang, J. Li, W. Fu, Z. Zhang, G. Johnson, X. Lv, Y. Zhang, S. Zhang and F. Dong, Electrocatalytic hydrodechlorination of 2,4-dichlorophenol over palladium nanoparticles and its pH-mediated tug-of-war with hydrogen evolution, *Chem. Eng. J.*, 2018, **348**, 26–34.

5 N. Sun, Y. Qu, S. Chen, R. Yan, M. Humayun, Y. Liu, L. Bai, L. Jing and H. Fu, Efficient photodecomposition of 2,4-dichlorophenol on recyclable phase-mixed hierarchically structured $Bi_2O_3$ coupled with phosphate-bridged nano-$SnO_2$, *Environ. Sci.: Nano*, 2017, **4**, 1147–1154.

6 B. Cojocaru, V. Andrei, M. Tudorache, F. Lin, C. Cadigan, R. Richards and V. I. Parvulescu, Enhanced photo-degradation of bisphenol pollutants onto gold-modified photocatalysts, *Catal. Today*, 2017, **284**, 153–159.

7 Y. Feng, L. Yang, J. Liu and B. E. Logan, Electrochemical technologies for wastewater treatment and resource reclamation, *Environ. Sci.: Water Res. Technol.*, 2016, **2**, 800–831.

8 H. Bai, J. Juay, Z. Liu, X. Song, S. S. Lee and D. D. Sun, Hierarchical $SrTiO_3$/$TiO_2$ nanofibers heterostructures with high efficiency in photocatalytic $H_2$ generation, *Appl. Catal., B*, 2012, **125**, 367–374.

9 M. G. Peleyeju and O. A. Arotiba, Recent trend in visible-light photoelectrocatalytic systems for degradation of organic contaminants in water/wastewater, *Environ. Sci.: Water Res. Technol.*, 2018, **4**, 1389–1411.

10 P. Calza, P. Avetta, G. Rubulotta, M. Sangermano and E. Laurenti, $TiO_2$-soybean peroxidase composite materials as a new photocatalytic system, *Chem. Eng. J.*, 2014, **239**, 87–92.

11 C. Lin, Y. Song, L. Cao and S. Chen, Effective photocatalysis of functional nanocomposites based on carbon and $TiO_2$ nanoparticles, *Nanoscale*, 2013, **5**, 4986–4992.

12 J. Ng, S. Xu, X. Zhang, H. Y. Yang and D. D. Sun, Hybridized nanowires and cubes: a novel architecture of a heterojunctioned $TiO_2$/$SrTiO_3$ thin film for efficient water splitting, *Adv. Funct. Mater.*, 2010, **20**, 4287–4294.

13 S. Gora, A. Sokolowski, M. Hatat-Fraile, R. Liang, Y. N. Zhou and S. Andrews, Solar photocatalysis with modified $TiO_2$ photocatalysts: effects on NOM and disinfection byproduct formation potential, *Environ. Sci.: Water Res. Technol.*, 2018, **4**, 1361–1376.

14 Z. Zhao, X. Zhang, G. Zhang, Z. Liu, D. Qu, X. Miao, P. Feng and Z. Sun, Effect of defects on photocatalytic activity of rutile $TiO_2$ nanorods, *Nano Res.*, 2015, **8**, 4061–4071.

15 B. K. Mutuma, G. N. Shao, W. D. Kim and H. T. Kim, Sol–gel synthesis of mesoporous anatase-brookite and anatase-brookite-rutile $TiO_2$ nanoparticles and their photocatalytic properties, *J. Colloid Interface Sci.*, 2015, **442**, 1–7.

16 B. Zhao, L. Lin and D. He, Phase and morphological transitions of titania/titanate nanostructures from an acid to an alkali hydrothermal environment, *J. Mater. Chem. A*, 2013, **1**, 1659–1668.

17 S. M. El-Sheikh, T. M. Khedr, G. Zhang, V. Vogiazi, A. A. Ismail, K. O'Shea and D. D. Dionysiou, Tailored synthesis of anatase–brookite heterojunction photocatalysts for degradation of cylindrospermopsin under UV-vis light, *Chem. Eng. J.*, 2017, **310**, 428–436.

18 S. Park, S. Kim, H. J. Kim, C. W. Lee, H. J. Song, S. W. Seo, H. K. Park, D. W. Kim and K. S. Hong, Hierarchical assembly of $TiO_2$-$SrTiO_3$ heterostructures on conductive $SnO_2$ backbone nanobelts for enhanced photoelectrochemical and photocatalytic performance, *J. Hazard. Mater.*, 2014, **275**, 10–18.

19 W. Zhang, G. Li, H. Liu, J. Chen, S. Ma and T. An, Micro/nano-bubble assisted synthesis of Au/$TiO_2$@CNTs composite photocatalyst for photocatalytic degradation of gaseous styrene and its enhanced catalytic mechanism, *Environ. Sci.: Nano*, 2019, **6**, 948–958.

20 S. Ali, Z. Li, S. Chen, A. Zada, I. Khan, I. Khan, W. Ali, S. Shaheen, Y. Qu and L. Jing, Synthesis of activated carbon-supported $TiO_2$-based nano-photocatalysts with well recycling for efficiently degrading high-concentration pollutants, *Catal. Today*, 2019, **335**, 557–564.

21 R. K. Sonker, B. Yadav, V. Gupta and M. Tomar, Fabrication and characterization of ZnO-$TiO_2$-PANI (ZTP) micro/

nanoballs for the detection of flammable and toxic gases, *J. Hazard. Mater.*, 2019, **370**, 126–137.

22 M. Sun, Y. Kong, Y. Fang, S. Sood, Y. Yao, J. Shi and A. Umar, Hydrothermal formation of N/$Ti^{3+}$ codoped multiphasic (brookite-anatase-rutile) $TiO_2$ heterojunctions with enhanced visible light driven photocatalytic performance, *Dalton Trans.*, 2017, **46**, 15727–15735.

23 R. Kaplan, B. Erjavec, G. Dražić, J. Grdadolnik and A. Pintar, Simple synthesis of anatase/rutile/brookite $TiO_2$ nanocomposite with superior mineralization potential for photocatalytic degradation of water pollutants, *Appl. Catal., B*, 2016, **181**, 465–474.

24 A. Kogo, Y. Sanehira, M. Ikegami and T. Miyasaka, Brookite $TiO_2$ as a low-temperature solution-processed mesoporous layer for hybrid perovskite solar cells, *J. Mater. Chem. A*, 2015, **3**, 20952–20957.

25 J. Jin, S. Chen, J. Wang, C. Chen and T. Peng, $SrCO_3$-modified brookite/anatase $TiO_2$ heterophase junctions with enhanced activity and selectivity of $CO_2$ photoreduction to $CH_4$, *Appl. Surf. Sci.*, 2019, **476**, 937–947.

26 A. Truppi, F. Petronella, T. Placido, V. Margiotta, G. Lasorella, L. Giotta, C. Giannini, T. Sibillano, S. Murgolo and G. Mascolo, Gram-scale synthesis of UV-vis light active plasmonic photocatalytic nanocomposite based on $TiO_2$/Au nanorods for degradation of pollutants in water, *Appl. Catal., B*, 2019, **243**, 604–613.

27 A. Villa, N. Dimitratos, C. E. Chan-Thaw, C. Hammond, G. M. Veith, D. Wang, M. Manzoli, L. Prati and G. J. Hutchings, Characterisation of gold catalysts, *Chem. Soc. Rev.*, 2016, **45**, 4953–4994.

28 Y. Ma, K. Kobayashi, Y. Cao and T. Ohno, Development of visible-light-responsive morphology-controlled brookite $TiO_2$ nanorods by site-selective loading of AuAg bimetallic nanoparticles, *Appl. Catal., B*, 2019, **245**, 681–690.

29 S. Horikoshi, S. Sakamoto and N. Serpone, Formation and efficacy of $TiO_2$/AC composites prepared under microwave irradiation in the photoinduced transformation of the 2-propanol VOC pollutant in air, *Appl. Catal., B*, 2013, **140**, 646–651.

30 I. Velo-Gala, J. López-Peñalver, M. Sánchez-Polo and J. Rivera-Utrilla, Role of activated carbon surface chemistry in its photocatalytic activity and the generation of oxidant radicals under UV or solar radiation, *Appl. Catal., B*, 2017, **207**, 412–423.

31 T. N. Pham, D. Shi, T. Sooknoi and D. E. Resasco, Aqueous-phase ketonization of acetic acid over Ru/$TiO_2$/carbon catalysts, *J. Catal.*, 2012, **295**, 169–178.

32 X. Fu, H. Yang, H. Sun, G. Lu and J. Wu, The multiple roles of ethylenediamine modification at $TiO_2$/activated carbon in determining adsorption and visible-light-driven photoreduction of aqueous Cr(VI), *J. Alloys Compd.*, 2016, **662**, 165–172.

33 Z. Li, Y. Luan, Y. Qu and L. Jing, Modification strategies with inorganic acids for efficient photocatalysts by promoting the adsorption of $O_2$, *ACS Appl. Mater. Interfaces*, 2015, **7**, 22727–22740.

34 Y. Qin, G. Li, Y. Gao, L. Zhang, Y. S. Ok and T. An, Persistent free radicals in carbon-based materials on transformation of refractory organic contaminants (ROCs) in water: a critical review, *Water Res.*, 2018, **137**, 130–143.

35 P. Agnès, C. Chanèac, T. Elisabeth, M. Lèo and J. P. Jolivet, Synthesis of brookite $TiO_2$ nanoparticles by thermolysis of $TiCl_4$ in strongly acidic aqueous media, *J. Mater. Chem.*, 2001, **11**, 1116–1121.

36 J. Lin, B. Wang, W. D. Sproul, Y. Ou and I. Dahan, Anatase and rutile $TiO_2$ films deposited by arc-free deep oscillation magnetron sputtering, *J. Phys. D: Appl. Phys.*, 2013, **46**, 084008.

37 X. Liu, Y. Li, D. Deng, N. Chen, X. Xing and Y. Wang, A one-step nonaqueous sol-gel route to mixed-phase $TiO_2$ with enhanced photocatalytic degradation of rhodamine B under visible light, *CrystEngComm*, 2016, **18**, 1964–1975.

38 L. Jiang, Y. Li, H. Yang, Y. Yang, J. Liu, Z. Yan, X. Long, J. He and J. Wang, Low-Temperature Sol-Gel Synthesis of Nitrogen-Doped Anatase/Brookite Biphasic Nanoparticles with High Surface Area and Visible-Light Performance, *Catalyst*, 2017, **7**, 376.

39 W. He, J. Cai, X. Jiang, J.-J. Yin and Q. Meng, Generation of reactive oxygen species and charge carriers in plasmonic photocatalytic Au@$TiO_2$ nanostructures with enhanced activity, *Phys. Chem. Chem. Phys.*, 2018, **20**, 16117–16125.

40 X. Liu, Y. Li, S. Peng, G. Lu and S. Li, Modification of $TiO_2$ with sulfate and phosphate for enhanced eosin Y-sensitized hydrogen evolution under visible light illumination, *J. Phys. D: Appl. Phys.*, 2013, **12**, 1903–1910.

41 Y. Luan, Y. Feng, H. Cui, Y. Cao and L. Jing, Enhanced Photocatalytic Activity of P25 $TiO_2$ after Modification with Phosphate-Treated Porous $SiO_2$, *ChemPlusChem*, 2014, **79**, 1271–1277.

42 Y. Liu, Y. Zhu, J. Xu, X. Bai, R. Zong and Y. Zhu, Degradation and mineralization mechanism of phenol by $BiPO_4$ photocatalysis assisted with $H_2O_2$, *Appl. Catal., B*, 2013, **142**, 561–567.

43 E. Grabowska, M. Marchelek, T. Klimczuk, W. Lisowski and A. Zaleska-Medynska, $TiO_2$/$SrTiO_3$ and $SrTiO_3$ microspheres decorated with Rh, Ru or Pt nanoparticles: Highly UV-vis responsible photoactivity and mechanism, *J. Catal.*, 2017, **350**, 159–173.

44 Y. Zhang, Z. Shen, Z. Xin, Z. Hu and H. Ji, Interfacial charge dominating major active species and degradation pathways: an example of carbon based photocatalyst, *J. Colloid Interface Sci.*, 2019, **554**, 743–751.